Science of the Total Environment 820 (2022) 153324

Contents lists available at ScienceDirect

Science of the Total Environment

journal homepage: www.elsevier.com/locate/scitotenv

Characterizing the distinct modulation of future emissions on summer ozone concentrations between urban and rural areas over China

Xinran Zeng [a], Yang Gao [b,*], Yuhang Wang [c,*], Mingchen Ma [b], Junxi Zhang [d], Lifang Sheng [a]

[a] College of Oceanic and Atmospheric Sciences, Ocean University of China, Qingdao 266100, China
[b] Frontiers Science Center for Deep Ocean Multispheres and Earth System, and Key Laboratory of Marine Environment and Ecology, Ministry of Education, Ocean University of China, Qingdao National Laboratory for Marine Science and Technology, Qingdao 266100, China
[c] School of Earth and Atmospheric Sciences, Georgia Institute of Technology, Atlanta, GA 30332, USA
[d] State Key Laboratory of Clean Energy, Department of Energy Engineering, Zhejiang University, Hangzhou, 310027, China

HIGHLIGHTS

- Suburban-rural MDA8 ozone concentrations are higher than that in urban China.
- The urban-rural ozone contrast at present is reversed with reduced emission in future.
- The changes in future ozone exceedance largely mimic that of MDA8 ozone concentration.
- Higher future ozone in urban than rural deserves more attention due to urbanization.

GRAPHICAL ABSTRACT

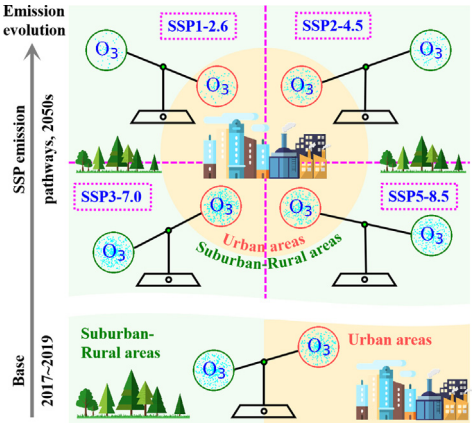

ARTICLE INFO

Article history:
Received 8 December 2021
Received in revised form 17 January 2022
Accepted 18 January 2022
Available online 21 January 2022

Editor: Hai Guo

Keywords:
Urban and suburban-rural areas
MDA8 ozone concentrations
SSPs
Ozone exceedance

ABSTRACT

Previous studies on ozone pollution primarily focus on the characterization of ozone on a large regional scale, yet much less attention has been paid towards the contrast between urban and surrounding suburban-rural areas. As anthropogenic emissions are projected to decrease in the coming decades, the evolutions of ozone concentrations over urban and suburban-rural areas are compared using the Community Multiscale Air Quality (CMAQ) model coupled with the Weather Research and Forecasting (WRF). The top 25 city clusters are firstly identified across China based on the amount of NO_x emissions and population size. At present, the averages of maximum daily 8-h (MDA8) ozone concentrations over the suburban-rural areas (65.74 ppbv) among these city clusters are higher than the corresponding urban areas (62.00 ppbv). The projections in 2050s depend on the scenarios. Under the Shared Socioeconomic Pathways (SSPs) scenarios such as SSP1-2.6, SSP2-4.5 and SSP5-8.5 indicative of primary decreases in anthropogenic emissions, the mean MDA8 ozone concentrations in suburban-rural areas decrease more than urban areas. In contrast, the gap of higher MDA8 ozone concentrations in suburban-rural than urban areas increases under SSP3-7.0 concomitant with increase in anthropogenic emissions. The strongest response to emission changes is found in SSP1-2.6, in which anthropogenic emission reduction leads to lower MDA8 ozone concentrations in the suburban-rural than urban areas, reversing the present state of higher ozone concentrations in the suburban-rural areas. The feature abovementioned regarding changes of mean MDA8 ozone concentrations is largely reproduced in the response of ozone exceedance. The finding highlights different efficacies of anthropogenic emissions in urban from suburban-rural areas. In a region

* Corresponding authors.
E-mail addresses: yanggao@ouc.edu.cn (Y. Gao), yuhang.wang@eas.gatech.edu (Y. Wang).

http://dx.doi.org/10.1016/j.scitotenv.2022.153324

like China where the population density is much higher in urban than suburban-rural regions, the benefit of ozone reduction due to large emission reductions (e.g., SSP1-2.6) is diminished to some extent because the effect is larger in suburban-rural areas.

1. Introduction

Tropospheric ozone is an important trace gas in the atmosphere, and it is mainly generated by a sequence of complicated photochemical reactions of volatile organic compounds (VOC_s) and nitrogen oxides (NO_x) in the presence of sunlight (Atkinson, 2000; Chameides and Walker, 1973; Fishman and Crutzen, 1978; Sillman, 1999). As a strong oxidant distributed in the troposphere, high concentration near-surface ozone can not only exert adverse impacts on human health but also cause harmful effects on the growth of plants and ecosystem productivity (Booker et al., 2009; Fann et al., 2012; Fowler et al., 2009; Lin et al., 2018; Yang et al., 2021). Particularly over China, a number of studies have investigated the spatial and temporal characteristics of surface ozone concentrations (Gao et al., 2021; Gaudel et al., 2018; Li et al., 2020; Lu et al., 2020; Ma et al., 2019; Tang et al., 2009; Yang et al., 2020), indicative of persistent increase of ozone concentrations over majority of areas over China in summer recently.

Although the emissions of ozone precursors tend to be concentrated in urban areas resulting from highly developed industry, mobile vehicles, dense population, etc., the ozone concentrations are often found to be higher over suburban-rural areas instead (Huang et al., 2018; Li et al., 2011; Tong et al., 2017; Zhang et al., 2008; Zheng et al., 2010). For instance, during Regional Integrated Experiments of Air Quality over Pearl River Delta in October 2004, the observed ozone concentrations over the rural areas are higher than that over urban attributable to higher ozone production efficiency therein (Zhang et al., 2008). This phenomenon is consistently emerged in a few other locations, including the city of Ningbo over the Yangtze River Delta region (Tong et al., 2017), Tianjin over North China Plain (Han et al., 2013), as well as India (Kumar et al., 2014; Londhe et al., 2008) and Spain (Duenas et al., 2004).

In contrast, the interannual variations of ozone concentrations over urban, suburban and rural areas may depict distinct characteristics. It has been indicated that the maximum daily 8-h (MDA8) O_3 concentrations over suburban increase at a rate of 32% higher than that over urban area in Shanghai from 2006 to 2015 (Xu et al., 2019), and the annual mean ozone concentration increasing rate over rural Beijing is almost twice as high as that of a site in urban Beijing from 2006 to 2013 (Zhang et al., 2015). In contrast, a more recent study implies an opposite pattern with higher increase rate over urban than suburban and rural sites in Shenzhen during 2011–2017 (Huang et al., 2018). The contrast is likely to be induced by differences in the emission changes, particularly of NO_x emission increase in the earlier period and decrease recently (Li et al., 2017b), as well as the concomitant NO titration effect, which implies the complexity in the modulation of emissions changes on ozone concentration over urban, suburban and rural areas.

In addition to the studies focusing on the historical period, a number of studies have investigated the changes of ozone concentrations over China under future emission changes (Lee et al., 2015; Liu et al., 2013; Wang et al., 2013; Zhu and Liao, 2016). For example, under the Special Report on Emissions Scenarios (SRES) A1B scenario, by maintaining the meteorology at the present level and increasing emissions, the afternoon surface ozone concentrations are projected to increase on average of 12.8 ppbv in fall over South China (Liu et al., 2013) and 11.6 ppbv in summer across China (Wang et al., 2013). In contrast, under the scenario of representative concentration pathways (RCP) 2.6, a decrease of 4–10 ppbv is projected over majority of China by 2050 due to large emission reductions when meteorological conditions is fixed at the year of 2010 (Zhu and Liao, 2016). The Chinese government recently proposed the goal of carbon neutrality by 2060 (Cai et al., 2021), indicative of potentially substantial decrease in anthropogenic emissions. Nevertheless, how ozone concentrations over urban and suburban-rural areas in China response to the emission changes remains unclear.

To this end, using regional climate and air quality model Weather Research and Forecasting (WRF) model version 3.8.1 coupled with Community Multiscale Air Quality (CMAQ) model version 5.2, we first comprehensively evaluate the contrast in the ozone concentrations between urban and rural areas in China. This is followed by an assessment of changes in the summer ozone concentrations in 2050s over China owing to anthropogenic emission changes under four shared socioeconomic pathways (SSPs) (SSP1-2.6, SSP2-4.5, SSP3-7.0, and SSP5-8.5), with a special focus on the comparison of responses between urban and suburban-rural areas.

2. Method

2.1. Model configurations

The regional climate model WRF version 3.8.1 is used to simulate the meteorological conditions, with modeling domain centered at 34° N, 110° E and two true latitudes of 25° N and 40° N, covering the entire China and several surrounding countries and regions (Fig. 1). The horizontal spatial resolution is 36 km × 36 km and number of vertical layers is 34 with model top at 50 hPa. The physics options used in this study are mostly the same as those in our previous studies (Ma et al., 2019; Yan et al., 2021), including the Morrison microphysics scheme (Morrison et al., 2009), the Rapid Radiation Transfer Model Global (RRTMG) for long- and short-wave radiation (Iacono et al., 2008; Morcrette et al., 2008), the unified Noah land surface model (Chen and Dudhia, 2001) and the Grell-Freitas cumulus parameterization scheme (Grell and Freitas, 2014). For planetary boundary layer scheme, the Yonsei University (YSU) (Hong et al., 2006) is selected based on the sensitivity test showing an improved performance using YSU scheme in comparison to other schemes such as Mellor-Yamada-Janjic (MYJ) scheme (Janjić, 1990; Janjić, 1994; Mellor and Yamada, 1982), detailed in Section 3. The initial and boundary conditions for WRF simulation are taken from the NCEP Climate Forecast System Reanalysis (CFSR) version 2 (Saha et al., 2014), with horizontal resolutions of 0.5° × 0.5°. The simulation period of WRF span the recent three-year from 2017 to 2019 when ozone pollution is much more severe relative to an earlier period (e.g., Fig. 4 in Ma et al. (2022)), and continuous simulations are conducted for each year with the previous December as spinup.

The air quality model CMAQ version 5.2 is used to simulate the ozone concentrations, sharing the same projection coordinate system as that of WRF. Carbon-bond version 6 (CB6) (Luecken et al., 2019) and Aerosol Module Version 6 (AERO6) (Murphy et al., 2017) are used as the gas-phase and aerosol chemistry mechanisms, respectively. The target of this study is to investigate the spatial and temporal characteristics in summer ozone concentrations, and continuous simulations from May 20 to August 31 with the first 12-day results discarded as spinup are conducted over each year of 2017–2019.

The chemical initial and boundary conditions are downscaled from the Model for Ozone and Related chemical Tracers, version 4 (MOZART-4) (Emmons et al., 2010), with detailed information in Ma et al. (2019). Anthropogenic emission inventory at spatial resolution of 0.25° × 0.25° is from Multi-resolution Emission Inventory for China (MEIC; http://www.meicmodel.org; last access: December 8, 2021) (Li et al., 2017a; Zheng et al., 2018). The hourly biogenic emissions are calculated using the Model of Emissions of Gases and Aerosols from Nature version 2.1 (MEGAN; (Guenther et al., 2012)), and monthly biomass burning emissions are from Global Fire Emissions Database Version 4 (GFED V4), with allocation factors provided to get the hourly emissions on each day (Randerson et al., 2017). Ship emissions are estimated from Shipping emission inventory model (SEIM; (Liu et al., 2016; Liu et al., 2019)). Since the non-methane volatile organic compounds (NMVOCs) are provided instead of

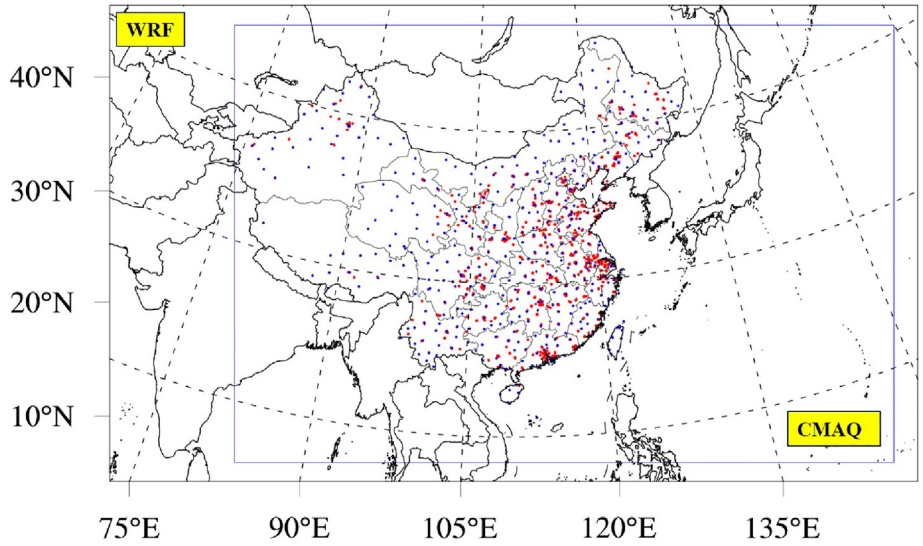

Fig. 1. The simulation domains of WRF and CMAQ. The simulations are in lambert conformal conic projection, with latitude and longitude lines in dashed gray. The red dots represent the environmental monitor stations from the China National Environmental Monitoring Centre and the blue dots present the meteorological observation stations from the National Climate Data Center (NCDC).

each VOC species in shipping emissions, allocation coefficients based on Lv et al. (2018) are applied to speciate NMVOCs to CB6 gas chemistry mechanism. While the year-specific data are used for biogenic and biomass burning emissions, the year of 2016 is used for anthropogenic emissions (MEIC) due to data availability.

Please note that the chemical boundary conditions of 2018 and 2019 are the same as 2017 due to the following reasons. The MOZART (https://www.acom.ucar.edu/wrf-chem/mozart.shtml; last access: December 8, 2021) results are available in 2017, but replaced by results from Community Atmosphere Model with Chemistry (CAM-chem) or Whole Atmosphere Community Climate Model (WACCM) thereafter. Our recent evaluation indicates large biases exist when using CAM-Chem or WACCAM particularly over the high-altitude areas near the western boundary, which is clearly indicated in Fig. S1 (panel iv of Fig. S1 (a) vs. panel viii of Fig. S1 (b)). Therefore, the MOZART simulations at the year of 2017 are used to provide the initial and boundary conditions among the three-year which should have negligible impact on the findings or conclusions revealed in this study in particular when the study area is not close to the boundaries (Yan et al., 2021).

The meteorological observational stations (approximately 400; blue dots) are taken from the National Climatic Data Center (NCDC, https://www.ncdc.noaa.gov/data-access/quick-links#dsi-3505; last access: December 8, 2021), including variables of air temperature and dew point at 2-m, wind speed and direction at 10-m. Hourly ozone monitoring data (in red), approximately 1700 sites, are obtained from the China National Environmental Monitoring Centre (CNEMC, http://www.pm25.in; last access: December 8, 2021).

2.2. Emission projections

In addition to the simulations during 2017–2019 driven by present emissions (defined as the case of Base), a few numerical experiments have been conducted by perturbing the emissions to project the possible future scenarios. Considering the previous scenarios such as RCPs (Van Vuuren et al., 2011) do not consider the socioeconomic narratives, a new set of climate scenarios which include assumptions of future socioeconomic development are designed and considered as SSPs of Coupled Model Intercomparison Project Phase 6 (CMIP6) (Gidden et al., 2019; Rao et al., 2017; Riahi et al., 2017). Four representative scenarios, e.g., SSP1-2.6, SSP2-4.5, SSP3-7.0, SSP5-8.5, are selected in this study to examine the effect of different emission pathways on the changes of ozone concentrations in urban and suburban-rural areas. The mid-century is set as the future period. The start year of SSPs is 2015, and monthly emissions are provided every 10 years starting from 2020 with a spatial resolution of $0.5^{\circ} \times 0.5^{\circ}$. Therefore, the future emissions used in regional air quality model CMAQ are acquired by applying a scaling ratio of emissions in 2050 to those in 2015 by country to Base. The meteorological conditions of future scenarios are the same as that of Base.

Please note that for the SSP scenarios, only anthropogenic emissions are projected to future period, with scaling ratio shown in Fig. 2, while the other emissions such as biomass burning, biogenic emissions maintain the same as Base scenario. Prior to the temporal ratio scaling, considering the differences in the emission species between SSPs and those used in CMAQ, they are firstly mapped from SSPs to that of the CMAQ model, such as gas, particulate matters (AERO6) and volatile organic compounds (VOCs) based on CB6 mechanism (Table 1). In another word, the ratio scaling of species in CMAQ is based on the corresponding species in SSPs, as is shown in Table 1. Considering the importance of anthropogenic VOC and NO_x emissions in modulating ozone concentrations, their changes are briefly discussed. For instance, most scenarios indicate the same sign of increase (SSP3-7.0) or decrease (SSP5-8.5, SSP1-2.6) in both VOCs and NO_x emissions. In contrast, the VOC emissions increase whereas NO_x emissions decrease in SSP2-4.5. On average, the change rate in VOC_s (NO_x) are −84% (−69%), 10% (−53%), 32% (20%), −6% (−11%) respectively for SSP1-2.6, SSP2-4.5, SSP3-7.0 and SSP5-8.5, with negative sign meaning emission reduction in future.

2.3. Identification of urban and suburban-rural areas

The urban areas are often characterized by developed transportation, concentrated industry and dense population. To identify an urban area, the combination of anthropogenic NO_x emissions and population density is applied. The population data at the year of 2015 is available at https://sedac.ciesin.columbia.edu/ (last access: December 8, 2021). Specifically, NO_x emissions in summer are added together over each grid in China, and all grids are then sorted to find out those exceeding the 99th percentile, and similar methods are applied to population density. A grid with exceedance of 99th percentiles across China in both NO_x emissions and population density is considered an urban grid. An urban area (red in Fig. 3) is then defined by including all the grids adjacent to each other, and the grids surrounding the urban area are considered suburban-rural area (green in Fig. 3). The urban and surrounding suburban-rural area is considered as a city cluster, yielding a total of 25 city clusters. Among these city clusters, the emission intensity of NO_x and VOC_s are generally higher in urban

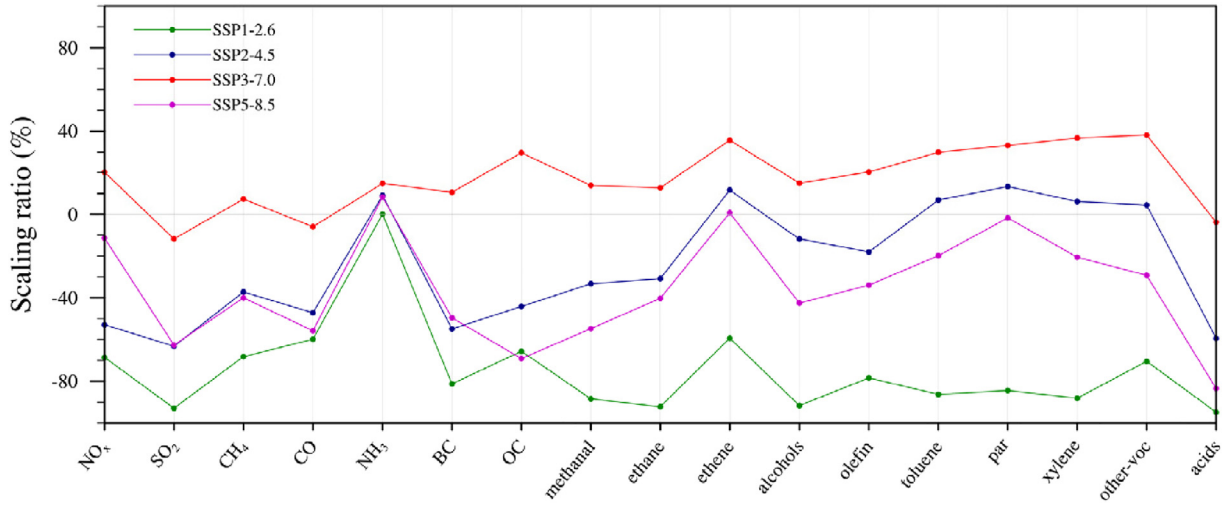

Fig. 2. Scaling ratio of emissions in 2050 to that in 2015 among different species in China under four SSPs.

than that of the suburban-rural areas, e.g., the summer NO_x and VOC emissions are 10.6 t/km^2 and 59.0 t/km^2 in urban areas, and 2.1 t/km^2 and 11.7 t/km^2 in suburban-rural areas.

3. Model evaluations

The model evaluation is first performed on the meteorological parameters during 2017–2019 including hourly air temperature at 2-m (T2), wind speed at 10-m (WS10) and wind direction at 10-m (WD10). The initial evaluation across the entire China indicates while reasonable performance of T2 is achieved, the bias in wind speed with PBL scheme of MYJ is relatively large (1.41 m/s) in comparison to the benchmark of 0.5 m/s (Emery et al., 2001). Considering that the PBL scheme is critical in modulating the meteorological parameters particularly the wind field (Hu et al., 2010) as well as the air quality (Jia and Zhang, 2020), another commonly used PBL scheme of YSU is applied to further test the capability in reproducing the wind vector, yielding an improved performance with mean bias of 0.84 m/s in China, consistent with the previous studies showing higher capability of YSU than MYJ in predicting the wind speed in selected regions and cases (Xie et al., 2012). The overall meteorological parameter comparisons between the WRF simulations with PBL scheme of YSU and observations over China and selected regions are provided in Table 2. The WRF model in general yields reasonable performance, within or quite close to the benchmark proposed by Emery et al. (2001). Please note that there is a relatively large bias in the gross error of wind direction compared to the benchmark, likely associated with the values particularly close to 0 or 360 degrees (Zhang et al., 2019).

The MDA8 ozone concentrations are evaluated against the observations over entire China, the urban and suburban-rural areas (e.g., 25 city clusters) defined above, shown in Fig. 4. The benchmarks are taken from EPA (2007), with the benchmarks of MFB, MFE, at 15%, 35%, respectively. The simulated MDA8 ozone concentrations well reproduce the observed values, and MFBs and MFEs over the three regions all satisfy the benchmarks.

Table 1
Mapping table between SSP species and CMAQ species.

SSPs	CMAQ
NO_x	NO_2
	NO
SO_2	SO_2
	SULF
CH_4	CH_4
CO	CO
NH_3	NH_3
BC	PEC
OC	POC
	PMOTHR
	PMC
NH_3	PNH4
NO_x	PNO_3
SO_2	PSO_4
Methanal	ALD2
	FORM
	ALDX
Ethane	ETHA
Ethene	ETH
Alcohols	ETOH
	MEOH
Olefin[a]	IOLE
	OLE
Toluene	TOL
par[b]	PAR
Xylene	XYLMN
Other-voc	UNR
Acids	AACD

[a] olefin = ethene + propene + other-alke.
[b] par = propane + butanes + pentanes + hexanes-pl.

4. Results and discussions

4.1. The MDA8 ozone concentrations in China under the Base and SSP scenarios

The spatial distributions of summer mean MDA8 ozone concentrations in Base (Fig. 5) show large spatial heterogeneity, depicting higher ozone concentrations in the northern and eastern flanks compared to that in the southern and western flanks. The changes among the four scenarios relative to Base show distinct characteristics. SSP3-7.0 yields the largest ozone increment, with positive values over almost the entire China, e.g., the mean and maximal increase reaches 2.3 ppbv and 8.1 ppbv, respectively. All the other three scenarios (SSP1-2.6, SSP2-4.5 and SSP5-8.5) show decrease of MDA8 ozone concentrations in majority of China, with largest mean national decrease at 9.2 ppbv under SS1-2.6. However, instead of a uniform decrease across the entire China, the ozone concentrations in the southwestern China increases at the scenarios of SSP2-4.5 and SSP5-8.5. This phenomenon is likely attributable to the persistent emission increases in northeastern India under SSP2-4.5 and SSP5-8.5, but decreases in SSP1-2.6. The transboundary effect is supported by previous studies showing the transport from India could clearly influence the air quality in southwestern China (Wang et al., 2013; Zhang et al., 2020). Moreover, the larger spatial invasion in SSP5-8.5 due possibly to the transport is well supported by the larger anthropogenic emission enhancement in India (e.g., 61% of NO_x

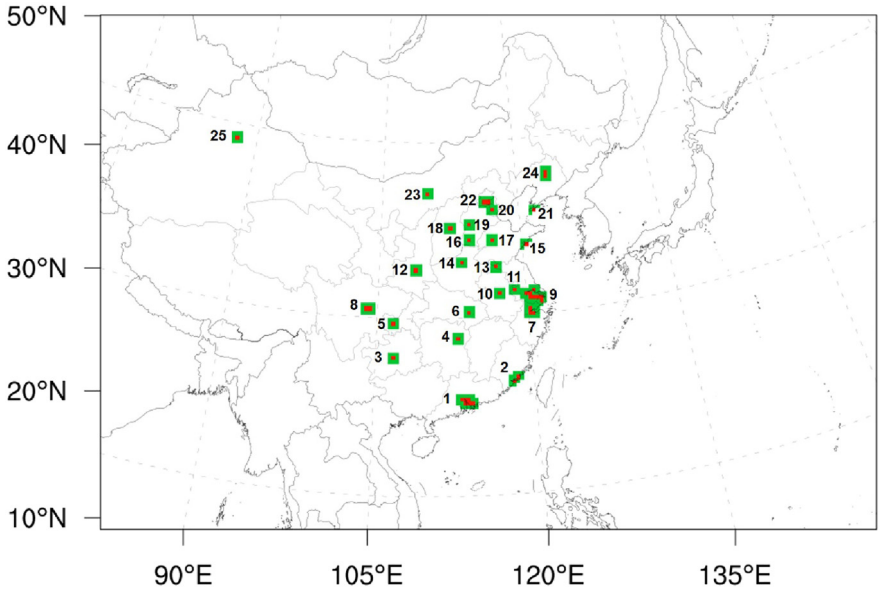

Fig. 3. Locations of urban and suburban-rural areas in China. The regions in red and green represent the urban and suburban-rural areas, with the numbers representing the city clusters from south to north China.

emissions) than that in SSP2-4.5 (e.g., 33% of NO_x emissions). Therefore, regional joint efforts may play pivotal roles in protecting air quality particularly over the borderline areas.

4.2. Changes of summer ozone exceedance over China under four SSP scenarios

The Technical Regulation on Ambient Air Quality Index (HJ633–2012) indicates ozone as a non-attainment pollutant (Class III or above) when MDA8 ozone is 160 μg m^{-3}, corresponding to 82 ppbv at 298 K and 1013 hPa, and a more stringent standard of 70 ppbv is suggested by National Ambient Air Quality Standards (NAAQS) of United States. An ozone exceedance day is defined as the MDA8 ozone concentration exceeding the criteria, and both criteria are applied in this study to examine how changes in emissions affect the ozone attainment.

Spatial distributions of ozone exceedance in summer for the scenarios of Base and SSPs, with MDA8 ozone concentration exceeding 82 ppbv and 70 ppbv are shown in Fig. 6 and Fig. S2, respectively. Consistent with the features of spatial heterogeneity in Fig. 5, approximately a third of summer days face ozone non-attainment over the pollution-prone regions such as North China Plain, much higher than majority of the other areas in China (Fig. 6a). In future, the emissions reduction (e.g., SSP1-2.6, SSP2-4.5, SSP 5-8.5) is concomitant with decrease in the ozone exceedance days (Fig. 6 c,d,f), weakening the spatial heterogeneity and particularly over SSP1-2.6, under which the exceedance days are mostly below 10 over China. In contrast, the emission increase in SSP3-7.0 triggers about 9 days increase on average. It is noteworthy that the changes in the ozone exceedances in southwestern China are relatively small in almost all four SSP scenarios, likely attributable to the transboundary transport, e.g., influence from India abovementioned (Fig. 5), and the stratospheric tropospheric transport (i.e., Lin et al. (2015) and Ni et al. (2019)).

To more clearly delineate the overall ozone exceedance in China, the probability distribution functions (PDFs) of MDA8 ozone concentrations are displayed in Fig. 6b, with the percentage exceedance to 82 ppbv and 70 ppbv in China shown on the top right. The percentage exceedance is calculated as the total exceedance days in three-summer across all grids divided by the total sample size, equivalent to the product of number of grids in China and days (e.g., three-summer, 276 days in this case). In Base, the ozone exceedance to 82 ppbv and 70 ppbv reaches 4.5% and 13.1%, respectively. The exceedance rates (Fig. 6b) of SSP1-2.6 (green), SSP2-4.5 (blue) and SSP5-8.5 (orange) are reduced resulting from emission reductions, characterized by notably shifts towards lower values in both the low-end and high-end tails of PDFs of MDA8 ozone concentrations. In contrast, under the scenario of SSP3-7.0 (magenta in Fig. 6b), the PDF of MDA8 ozone concentrations show clearly right shift, indicative aggravated ozone exceedance, i.e., 6.3% and 16.4% respectively, to 82 ppbv and 70 ppbv relative to Base.

Table 2
Evaluation of WRF model simulations.

		China	Selected regions[a]	Benchmarks
Air temperature at 2-m (°C)	Mean OBS[b]	24.21	27.11	
	Mean MODEL[c]	23.59	26.77	
	Mean Bias	−0.62	−0.34	≤ ±0.5
	Gross Error	2.68	2.17	≤2.0
Wind speed at 10-m (m/s)	Mean OBS	2.66	2.89	
	Mean MODEL	3.5	3.38	
	Mean Bias	0.84	0.48	≤ ±0.5
	Gross Error	1.65	1.42	
Wind direction at 10-m (°)	Mean OBS	174.84	160.75	
	Mean MODEL	171.81	159.71	
	Mean Bias	−3.03	−1.04	≤ ±10
	Gross Error	85.28	68.96	≤ 30

[a] Selected region represents all urban and suburban-rural areas.
[b] OBS indicates values from observations.
[c] MODEL indicates values from simulated results in WRF.

4.3. The MDA8 ozone concentrations over urban and suburban-rural areas

Fig. 7 shows the comparison of MDA8 ozone concentrations between the selected urban and suburban-rural areas, defined in Section 2.3. MDA8 ozone concentrations over all urban and suburban-rural grids are averaged separately first to retrieve spatial mean values for MDA8 ozone, NO_x and VOC concentrations on each day, and are displayed in Fig. 7 with colored dots indicative of MDA8 ozone concentrations as a function of VOC_s (abscissas; marked on top of each panel) and NO_x (ordinates). Please note concentrations of NO_x and VOC_s in both the urban and suburban-rural areas are divided into 50 bins. The first striking feature is a separation line (dashed black in Fig. 7 a-e, with top and bottom of the line shading in blue and red, respectively) can be clearly drawn along the Y axis, indicating that the maximal value of NO_x concentrations averaged over the suburban-rural areas (bottom portion of each panel in Fig. 7) during the

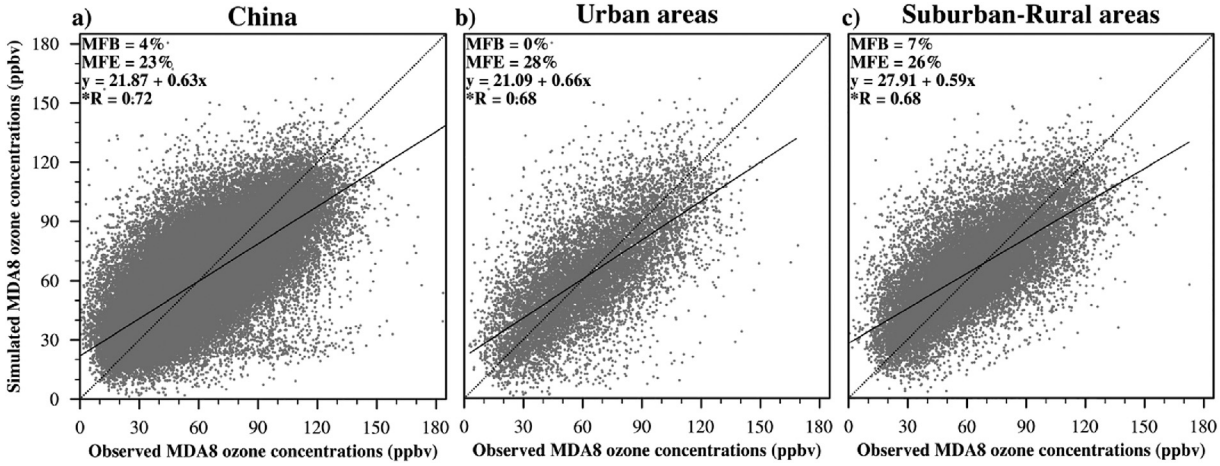

Fig. 4. The comparison of MDA8 ozone concentrations between CMAQ simulations and observations. Shown are linear regressions over entire China, urban (red in Fig. 3) and suburban-rural (green in Fig. 3) areas in summer 2017–2019, with regression lines in solid black and 1:1 line in dashed black. The numbers located at the top left of each panel indicate the statistical metrics including mean fractional bias (MFB), mean fractional error (MFE) and correlation coefficient (R). The asterisk on the top left of R indicative of statistical significance at the 95% confidence level. (For interpretation of the references to colour in this figure legend, the reader is referred to the web version of this article.)

three-summer 2017–2019 are smaller than the minimal one over the urban areas (top portion of each panel in Fig. 7), which is understandable as part of the constraint in the definition (Section 2.3). The high and low NO_x concentration contrast in urban and suburban-rural areas is supported by the measurement data as well.

In Base (Fig. 7a), the summer mean MDA8 ozone concentrations over urban areas are 62.00 ppbv (blue bar in Fig. 7a), lower with statistical significance ($P < 0.05$) than that of the suburban-rural areas with the value of 65.74 ppbv (red bar in Fig. 7a). In the urban areas of Base (top portion of Fig. 7a), the MDA8 ozone concentrations become larger with the increase of VOC concentrations, but smaller with the increase of NO_x concentrations, exhibiting the effect of NO titration and consistent with the relationship shown in O_3-NO_x-VOC Empirical kinetic modeling approach (EKMA) diagram in previous studies (Gao et al., 2021; Qu et al., 2020; Tan et al., 2018). The ozone contrasts between urban and suburban-rural areas have also been documented in Tong et al. (2017), indicating that lower ozone concentrations over urban areas are likely due to the influence of the NO titration compared with suburban-rural areas, through measurement over different types of stations in Ningbo from September 2014 to August 2015.

However, the dipole relationship in Base, characterized by lower MDA8 ozone concentrations in urban areas and higher concentrations in suburban-rural areas, is maintained under the emission scenario such as SSP3-7.0 with increase anthropogenic VOCs and NO_x, but reversed when emissions particularly of NO_x are largely reduced (e.g., SSP1-2.6 and SSP2-4.5), with an exception of SSP5-8.5, under which the MDA8 ozone concentrations in urban areas are lower than suburban-rural areas even when both VOC and NO_x emissions are reduced. The differences in the MDA8 ozone changes are tightly modulated by changes in the emissions of VOCs and NO_x. In SSP3-7.0, along with the emission increase, the ozone enhancement is even larger in the suburban-rural areas (3.46 ppbv; red bars in Fig. 7d vs. Fig. 7a) than that in urban areas (1.94 ppbv; blue bars in Fig. 7d vs. Fig. 7a), leading to strengthened contrast between them, primarily attributable to the comparable magnitudes of the increase in NO_x (19%) and VOC (16%) emissions plus the titration effect therein.

The mechanisms governing different behaviors, in MDA8 ozone concentration contrasts between urban and suburban-rural areas, among the scenarios of SSP5-8.5 and SSP1-2.6, SSP2-4.5 are likely as follows. In SSP5-8.5, relatively small anthropogenic NO_x emission reduction rate (11%) is indicative of possible existence of the NO titration which may thereby trigger the lower MDA8 ozone concentrations in urban compared to suburban-rural areas. Nevertheless, the reduction in NO_x emissions in SSP5-8.5 has weakened the NO titration to a certain extent, yielding a smaller gap between urban and suburban-rural area compared to Base (Fig. 7e vs. Fig. 7a), consistent with the discussions of O_3-NO_x-VOC EKMA diagram in Gao et al. (2021). When extra NO_x emissions are reduced in either SSP1-2.6 (69%) or SSP2-4.5 (53%) regardless of the changes in VOCs, the diminished or even disappeared NO titration effect, relative to Base, induces smaller magnitudes of ozone decreases in urban areas compared to suburban-rural areas, thereby leading to the reversal pattern of larger MDA8 ozone in urban areas (blue vs. red bars in Fig. 7b,c). This has important implications due to urbanizations and urban expansions, and it is expected to have more population living in urban areas (Bren d'Amour et al., 2017), and the large NO_x emission reduction, despite of ozone decrease, may pose higher threat to human beings in urban areas compared to suburban-rural in future, in the context of the MDA8 ozone concentration contrast therein.

4.4. The ozone exceedance over urban and suburban-rural areas

The ozone exceedance rates over the urban and suburban-rural areas are shown in the box-and-whisker plots in Fig. 8. The ozone exceedance rate is calculated over the urban (red in Fig. 3) and suburban-rural (green in Fig. 3) areas respectively for each city cluster. For each city cluster, calculation of ozone exceedance rate is first to count the number of days with MDA8 ozone concentration over each grid exceeding the threshold of 82 ppbv (Fig. 8) or 70 ppbv (Fig. S3), which is summed together and then divided by the total sample size, defined as the product of total days (276 days) in the three-summer and number of grids in either urban or suburban-rural area. It can be found that the mean exceedance rate of suburban-rural area is slightly higher than that of the urban area in Base, and the ratio of mean ozone exceedance rate in urban to that over suburban-rural areas is 0.98, consistent with the contrast in mean ozone concentrations (blue vs. red bars in Fig. 7a). This result is comparable to a previous study (Huang et al., 2018), which indicates that ozone exceedance rates of suburban-rural sites are higher than that of urban site from 2011 to 2017, based on observational data in Shenzhen, a city in southern China.

When the changes in emissions are considered, the signal in the changes of ozone exceedance rate are in general consistent with the findings revealed in the mean ozone, i.e., increased contrast between urban and suburban-rural areas in SSP3-7.0, and reversed relationship of higher ozone exceedance rate in urban and lower rate in suburban-rural areas in SSP1-2.6 and SSP2-4.5 (Fig. 7b, c, d vs. Fig. 8). Particularly, under the SSP1-2.6 close to carbon neutrality, the ozone exceedance rate in urban areas may be 72% larger than that of the suburban-rural areas, potentially posing greater human health risks considering urban expansions in future (Bren d'Amour et al., 2017).

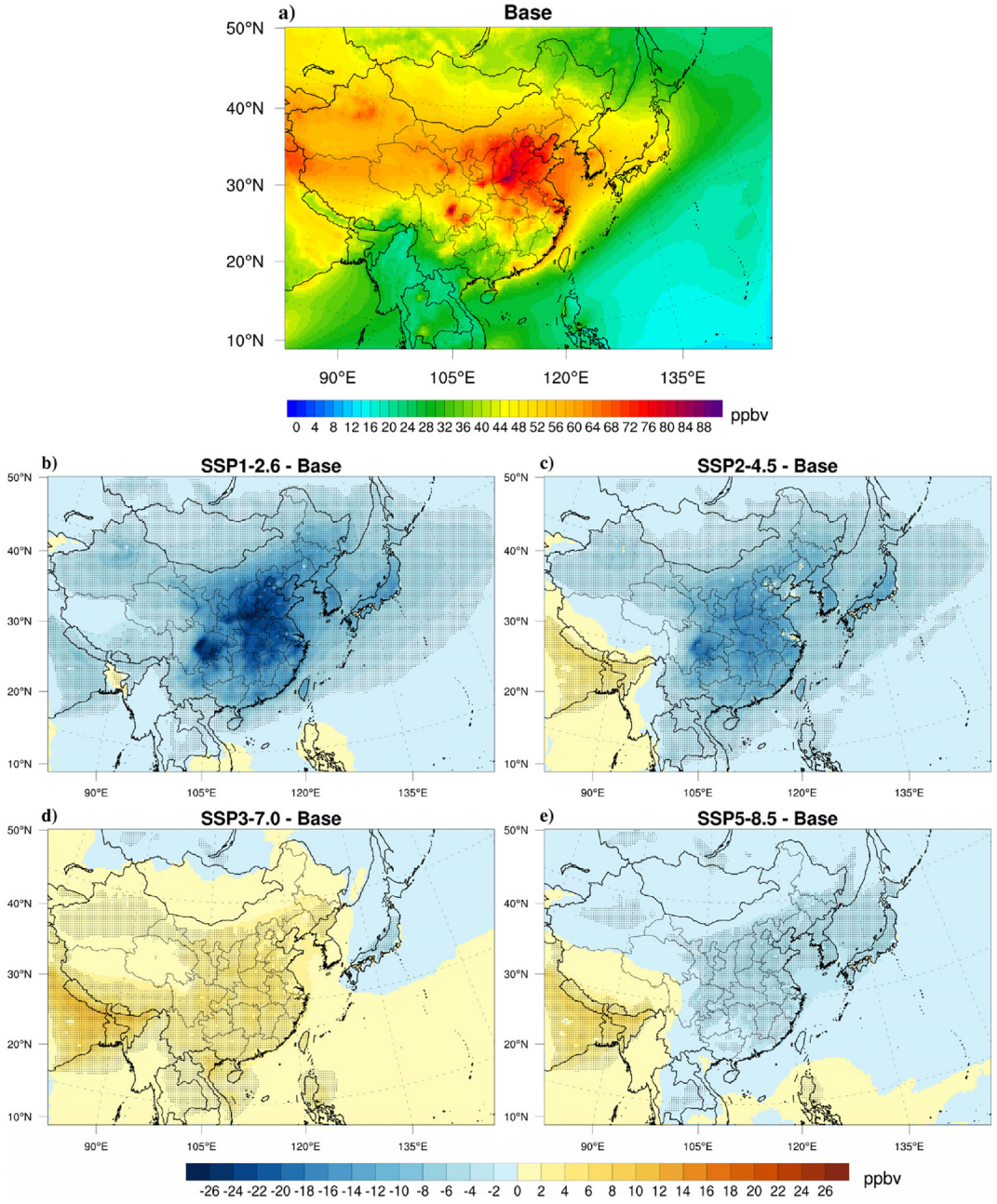

Fig. 5. Summer mean MDA8 ozone concentrations and its future changes. Shown are spatial distributions at (a) Base, and changes under the scenarios of (b) SSP1-2.6, (c) SSP2-4.5, (d) SSP3-7.0 and (e) SSP5-8.5. Black stippled areas indicate changes with statistical significance at 95% level based on Student's *t*-test.

Nevertheless, seemingly distinct characteristics emerge in SSP5-8.5. While the MDA8 ozone concentrations in suburban-rural areas maintain higher than that over urban areas in SSP5-8.5, comparable to but weakened contrasts than Base (Fig. 7a vs. Fig. 7e), the ozone exceedance rate reverses for SSP5-8.5, meaning higher exceedance rate in urban and lower in suburban-rural areas (Fig. 8), sharing the same signal as SSP1-2.6 and SSP2-4.5. Despite the signal reversal between ozone exceedance rates and concentrations in SSP5-8.5, it can be considered the expansion of the contrast weakening. In fact, the results based on the threshold of 70 ppbv (Fig. S3) do not show signal reversal, maintaining similar contrasts (higher rate in suburban-rural than urban areas) between SSP5-8.5 and Base, but the contrasts in SSP5-8.5 becomes smaller due to larger decrease of ozone exceedance rates over suburban-rural than urban areas. It is then understandable that the emergence of a reversal relationship in SSP5-8.5, with the threshold of 82 ppbv, is likely attributable to the relatively small differences in ozone exceedance rates between suburban-rural than urban areas in Base (Fig. 8), as well as the larger ozone exceedance rate decrease in suburban-rural areas.

Please note that the selection of urban grids is based on those exceeding the threshold of 99th percentile of anthropogenic NO_x emissions and population density in China, and sensitivity tests are done by applying different thresholds (e.g., a higher one of 99.5th and a lower one of 98th), which yields consistent results such as the contrast between urban and suburban-rural MDA8 ozone concentration and exceedance, but with an enhanced (weakened) magnitude under 99.5th (98th) percentile.

5. Conclusions and uncertainty discussions

This study applies the WRF-CMAQ model to investigate the future changes of summertime ozone air quality in China under the latest CMIP6

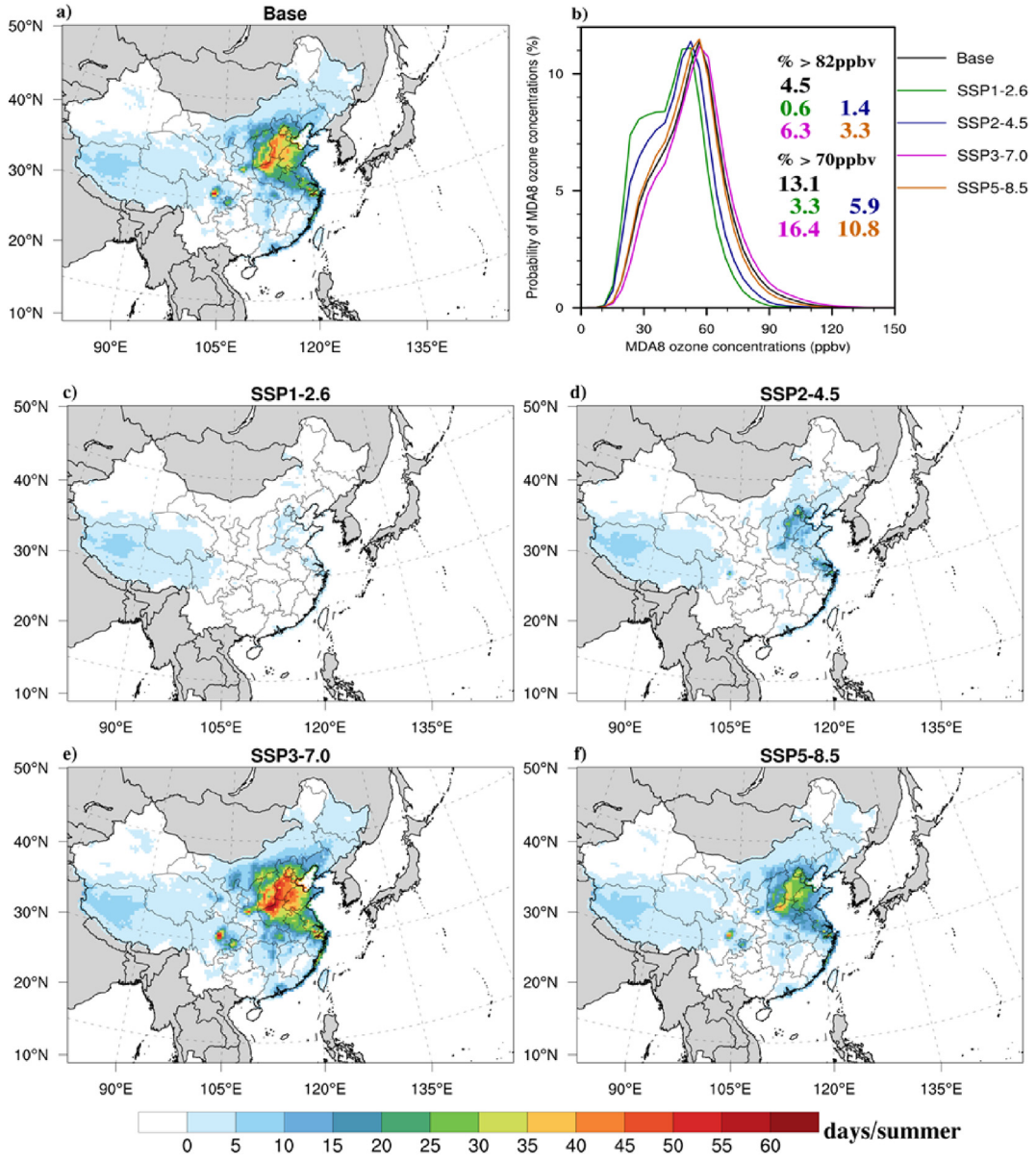

Fig. 6. Spatial distributions of summer mean ozone exceedance days and probability distribution function of summer MDA8 ozone concentrations in China. Shown are spatial distributions at (a) Base, (c) SSP1-2.6, (d) SSP2-4.5, (e) SSP3-7.0, (f) SSP5-8.5 with the threshold of 82 ppbv as well as (b) Probability density distributions of MDA8 ozone concentrations at Base and four SSP scenarios. In b), there are two sets of numbers in the figure legend, showing the ozone exceedances in China: the numbers below "% > 82 ppbv" show the percentage of MDA8 ozone concentrations exceeding 82 ppbv, and the number below "% > 70 ppbv" are for MDA8 ozone concentrations exceeding 70 ppbv under different scenarios.

emission pathways (SSP1-2.6, SSP2-4.5, SSP3-7.0, and SSP5-8.5). Particular attention is placed upon the differential responses over urban and suburban-rural areas.

By the comparison of the MDA8 ozone concentrations over China under Base and SSP scenarios, it is found that SSP1-2.6, which is close to the carbon neutrality scenario, has the best ozone reduction among the four SSP scenarios, with the mean decrement of 9.2 ppbv over China, followed by SSP2-4.5 at 6.1 ppbv, and SSP5-8.5 at 1.3 ppbv. The SSP3-7.0 scenario is worst for ozone air quality with an average increase of 2.3 ppbv over China. It is noted that the MDA8 ozone concentrations in parts of southwestern China show increases under SSP2-4.5 and SSP5-8.5 scenarios, which may be influenced in part by increasing NO_x emissions from Northeast India in these scenarios. The changes of ozone exceedance days over China under Base and SSP scenarios also indicated that SSP1-2.6 is the most favorable scenario for ozone air quality improvement, with average exceedance days less than 10 days over majority of China, and the SSP3-7.0 is the worst scenario, with more exceedance days than Base.

Through the analysis of the different responses of urban and suburban-rural areas under different SSP scenarios, we find that the changes of ozone concentrations in the suburban-rural areas are more sensitive to the changes of emissions than that of the urban areas. In Base, the concentrations of MDA8 ozone are higher in suburban-rural than that over urban areas, which reflects lower ozone concentrations with higher NO_x emissions (e.g, Qu et al. (2020)). As NO_x emissions are lower under SSP1-2.6 and SSP2-4.5 scenarios, ozone concentrations are lower in suburban-rural than urban region, reversing the urban-rural ozone difference in the Base. The average percentages of ozone exceedance days show similar characteristics. The urban to suburban-rural ratio of exceedance days in Base is 0.98 but increases to 1.72 and 1.63 under SSP1-2.6 and SSP2-4.5 scenarios, respectively. This is of great significance, and it is expected that more people will move to urban areas in China due continuing urbanization polices,

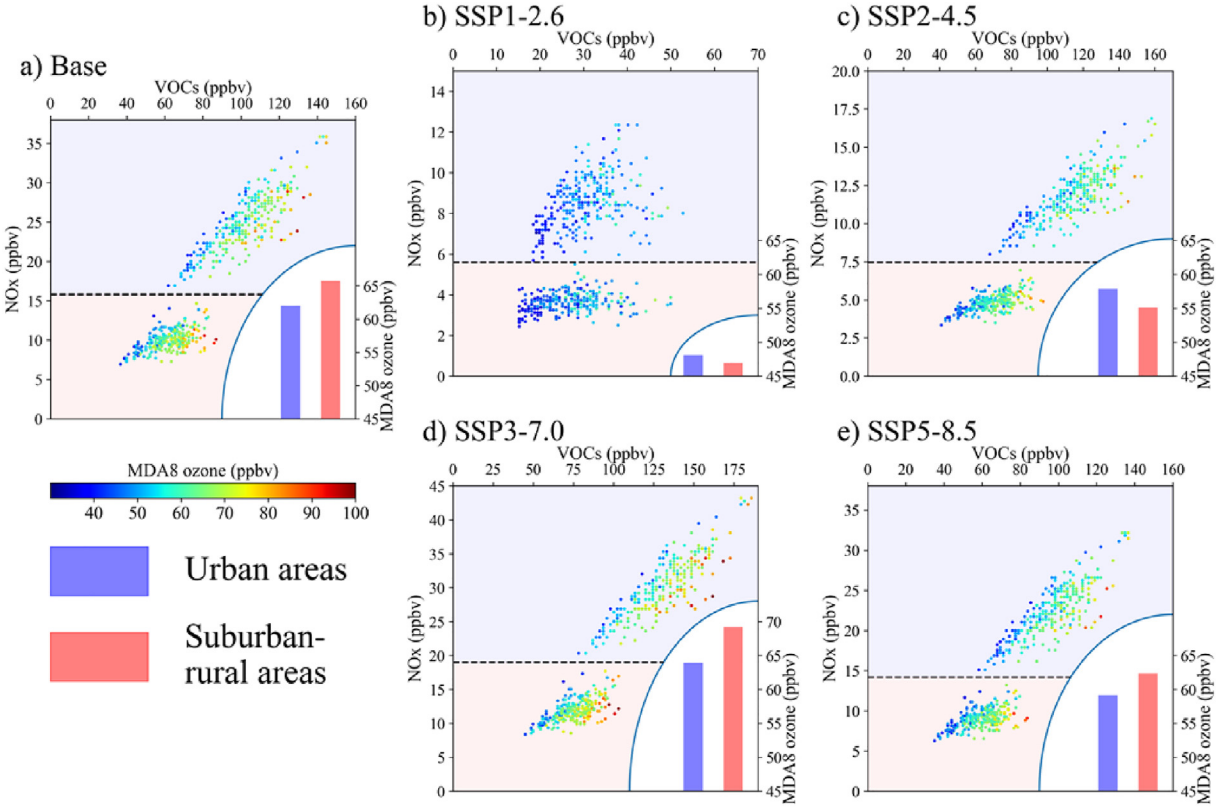

Fig. 7. The comparison of MDA8 ozone concentrations between the urban and suburban-rural areas. The colored dots are indicative of MDA8 ozone concentrations as a function of VOCs (abscissas; marked on top of each panel) and NO_x (ordinates) for Base (Fig. 7a) and four SSP scenarios (SSP1-2.6, SSP2-4.5, SSP3-7.0 and SSP5-8.5; Fig. 7b-e). Note that the concentrations of NO_x and VOCs are divided into 50 bins. A line (dashed black in Fig. 7 a-e) is drawn to separate the urban (top of the line, shading in blue) and suburban-rural (bottom of the line, shading in red) areas. Bar charts (right bottom of each panel) represent three-summer mean MDA8 ozone concentrations averaged over all urban (blue) or suburban-rural (red) grids under Base and SSPs.

while NO_x emission reductions may lead to higher ozone concentrations in urban than suburban-rural areas. In a region like China where the population density is much higher in urban than suburban-rural regions, the benefit of ozone reduction due to large emission reductions under the SSP1-2.6 scenario is diminished to some extent because the effect is larger in suburban-rural than urban areas.

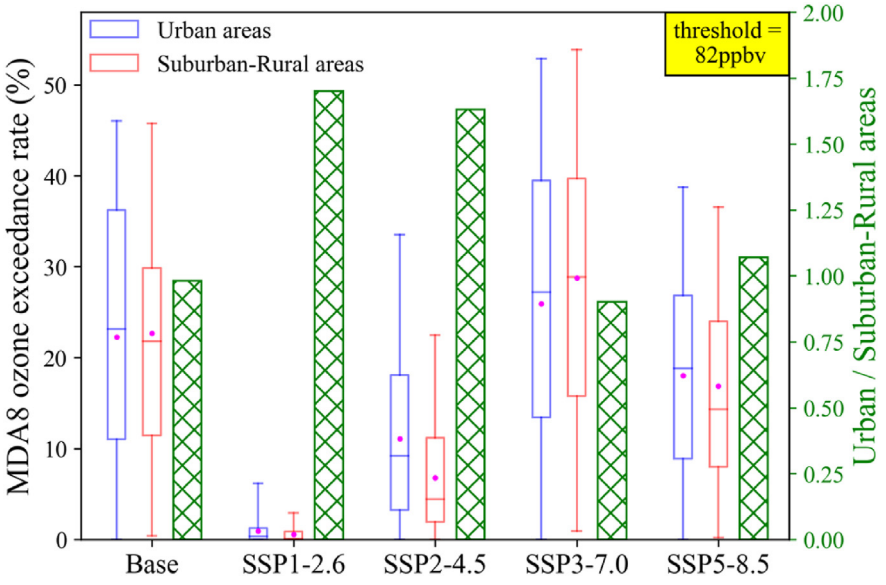

Fig. 8. The MDA8 ozone exceedance rates. Shown are results over the urban (red) and suburban-rural areas (blue) of the 25 city clusters in box-and-whisker plot, with the minimum and maximum (line end points), 25th and 75th percentile (boxes), medians (horizontal lines), and average (magenta points). and the ratio of mean MDA8 ozone exceedance rates over the urban to suburban-rural areas are shown in green hatched bars under Base and four SSP scenarios (SSP1-2.6, SSP2-4.5, SSP3-7.0 and SSP5-8.5) with the threshold of 82 ppbv.

There are a couple of uncertainties which deserve more investigations in future. First, the future scenarios are based on emission perturbations only while maintaining meteorological conditions at present. It is useful to make a comparison by conducting numerical experiments based on future meteorology under scenarios like SSPs, and future changes in meteorological parameters such as planetary boundary layer (Sánchez et al., 2007) may affect vertical ozone transport as well as surface ozone (Kalabokas et al., 2020; Kalabokas et al., 2015). Second, this study primarily focuses on summer ozone, whereas in southern China, ozone pollution is more prone to occur in other seasons such as fall (Shen et al., 2015; Situ et al., 2013), which deserves further investigation. Lastly, the soil NO_x (Lu et al., 2021), biogenic VOC emissions particularly from urban green spaces (Gao et al., 2022; Ma et al., 2022) as well as the synergic effect with anthropogenic emissions (Gao et al., 2021) on ozone formation are not considered, which may steer the future changes of ozone exceedance days in urban and suburban-rural regions and deserve more studies in future.

Data availability

The data used in this study is available upon request to the corresponding author (yanggao@ouc.edu.cn).

CRediT authorship contribution statement

Xinran Zeng: Formal analysis, Writing – original draft. **Yang Gao:** Conceptualization, Methodology, Writing – review & editing. **Yuhang Wang:** Methodology, Writing – review & editing. **Mingchen Ma:** Visualization. **Junxi Zhang:** Visualization. **Lifang Sheng:** Writing – review & editing.

Declaration of competing interest

The authors declare that they have no known competing financial interests or personal relationships that could have appeared to influence the work reported in this paper.

Acknowledgements

This research was supported by grants from the National Natural Science Foundation of China (42122039). The analysis was performed using the computing resources of Center for High Performance Computing and System Simulation, Pilot National Laboratory for Marine Science and Technology (Qingdao). Y.W. was supported by the National Science Foundation Atmospheric Chemistry Program.

Appendix A. Statistical parameters for evaluation model performance

The statistical metrics, used in the model evaluation, include Mean Bias, RMSE (root mean square error), Gross Error, MFB (mean fractional bias), MFE (mean fractional error) and R (correlation coefficient). Calculation of these metrics are shown below in Eqs. (A1)–(A6), where N is the total samples, MOD and OBS represent the corresponding values in model simulations and observations, respectively.

Mean Bias	$= \frac{1}{N}\sum_{i=1}^{N}(\mathbf{MOD_i} - \mathbf{OBS_i})$	(A1)
RMSE	$= \sqrt{\frac{1}{N}\sum_{i=1}^{N}(\mathbf{MOD_i} - \mathbf{OBS_i})^2}$	(A2)
Gross Error	$= \frac{1}{N}\sum_{i=1}^{N}\lvert\mathbf{MOD_i} - \mathbf{OBS_i}\rvert$	(A3)
MFB	$= \frac{2}{N}\sum_{i=1}^{N}\frac{(\mathbf{MOD_i} - \mathbf{OBS_i})}{(\mathbf{MOD_i} + \mathbf{OBS_i})} \times \mathbf{100}\%$	(A4)
MFE	$= \frac{2}{N}\sum_{i=1}^{N}\frac{\lvert\mathbf{MOD_i} - \mathbf{OBS_i}\rvert}{(\mathbf{MOD_i} + \mathbf{OBS_i})} \times \mathbf{100}\%$	(A5)
R	$= \frac{\sum_{i=1}^{N}[(\mathbf{MOD_i} - \overline{\mathbf{MOD}}) \times (\mathbf{OBS_i} - \overline{\mathbf{OBS}})]}{\sqrt{\sum_{i=1}^{N}(\mathbf{MOD_i} - \overline{\mathbf{MOD}})^2 \times \sum_{i=1}^{N}(\mathbf{OBS_i} - \overline{\mathbf{OBS}})^2}}$	(A6)

Appendix B. Supplementary data

Supplementary data to this article can be found online at https://doi.org/10.1016/j.scitotenv.2022.153324.

References

Atkinson, R., 2000. Atmospheric chemistry of VOCs and NOx. Atmos. Environ. 34, 2063–2101.
Booker, F., Muntifering, R., McGrath, M., Burkey, K., Decoteau, D., Fiscus, E., et al., 2009. The ozone component of global change: potential effects on agricultural and horticultural plant yield, product quality and interactions with invasive species. J. Integr. Plant Biol. 51, 337–351.
Bren d'Amour, C., Reitsma, F., Baiocchi, G., Barthel, S., Güneralp, B., Erb, K.-H., et al., 2017. Future urban land expansion and implications for global croplands. Proc. Natl. Acad. Sci. 114, 8939–8944.
Cai, B., Cao, L., Lei, Y., Wang, C., Zhang, L., Zhu, J., et al., 2021. China's carbon emission pathway under the carbon neutrality target. China Popul. Resour. Environ. 31, 25–32.
Chameides, W., Walker, J.C.G., 1973. A photochemical theory of tropospheric ozone. J. Geophys. Res. 78, 8751–8760.
Chen, F., Dudhia, J., 2001. Coupling an advanced land surface-hydrology model with the Penn State–NCAR MM5 modeling system. Part I: model implementation and sensitivity. Mon. Weather Rev. 129, 569–585.
Duenas, C., Fernandez, M.C., Canete, S., Carretero, J., Liger, E., 2004. Analyses of ozone in urban and rural sites in Malaga (Spain). Chemosphere 56, 631–639.
Emery, C., Tai, E., Yarwood, G., 2001. Enhanced meteorological modeling and performance evaluation for two Texas ozone episodes. Prepared for the Texas natural resource conservation commission, by ENVIRON International Corporation.
Emmons, L.K., Walters, S., Hess, P.G., Lamarque, J.F., Pfister, G.G., Fillmore, D., et al., 2010. Description and evaluation of the model for ozone and related chemical tracers, version 4 (MOZART-4). Geosci. Model Dev. 3, 43–67.
EPA, U., 2007. Guidance on the use of models and other analyses for demonstrating attainment of air quality goals for ozone, PM2. 5, and regional haze. US Environmental Protection Agency, Office of Air Quality Planning and Standards.
Fann, N., Lamson, A.D., Anenberg, S.C., Wesson, K., Risley, D., Hubbell, B.J., 2012. Estimating the national public health burden associated with exposure to ambient PM2.5 and ozone. Risk Anal. 32, 81–95.
Fishman, J., Crutzen, P.J., 1978. The origin of ozone in the troposphere. Nature 274, 855–858.
Fowler, D., Pilegaard, K., Sutton, M.A., Ambus, P., Raivonen, M., Duyzer, J., et al., 2009. Atmospheric composition change: ecosystems-atmosphere interactions. Atmos. Environ. 43, 5193–5267.
Gao, Y., Yan, F., Ma, M., Ding, A., Liao, H., Wang, S., et al., 2021. Unveiling the dipole synergic effect of biogenic and anthropogenic emissions on ozone concentrations. Sci. Total Environ. 151722.
Gao, Y., Ma, M., Yan, F., Su, H., Wang, S., Liao, H., et al., 2022. Impacts of biogenic emissions from urban landscapes on summer ozone and secondary organic aerosol formation in megacities. Sci. Total Environ. 814, 152654.
Gaudel, A., Cooper, O.R., Ancellet, G., Barret, B., Boynard, A., Burrows, J.P., et al., 2018. Tropospheric Ozone Assessment Report: Present-day distribution and trends of tropospheric ozone relevant to climate and global atmospheric chemistry model evaluation. 6.
Gidden, M.J., Riahi, K., Smith, S.J., Fujimori, S., Luderer, G., Kriegler, E., et al., 2019. Global emissions pathways under different socioeconomic scenarios for use in CMIP6: a dataset of harmonized emissions trajectories through the end of the century. Geosci. Model Dev. 12, 1443–1475.
Grell, G.A., Freitas, S.R., 2014. A scale and aerosol aware stochastic convective parameterization for weather and air quality modeling. Atmos. Chem. Phys. 14, 5233–5250.
Guenther, A.B., Jiang, X., Heald, C.L., Sakulyanontvittaya, T., Duhl, T., Emmons, L.K., et al., 2012. The model of emissions of gases and aerosols from nature version 2.1 (MEGAN2.1): an extended and updated framework for modeling biogenic emissions. Geosci. Model Dev. 5, 1471–1492.
Han, S.-Q., Zhang, M., Zhao, C.-S., Lu, X.-Q., Ran, L., Han, M., et al., 2013. Differences in ozone photochemical characteristics between the megacity Tianjin and its rural surroundings. Atmos. Environ. 79, 209–216.
Hong, S.-Y., Noh, Y., Dudhia, J., 2006. A new vertical diffusion package with an explicit treatment of entrainment processes. Mon. Weather Rev. 134, 2318–2341.
Hu, X.-M., Nielsen-Gammon, J.W., Zhang, F., 2010. Evaluation of three planetary boundary layer schemes in the WRF model. J. Appl. Meteorol. Climatol. 49, 1831–1844.
Huang, D., Li, Q., Wang, X., Li, G., Sun, L., He, B., et al., 2018. Characteristics and trends of ambient ozone and nitrogen oxides at urban, suburban, and rural sites from 2011 to 2017 in Shenzhen, China. Sustainability 10.
Iacono, M.J., Delamere, J.S., Mlawer, E.J., Shephard, M.W., Clough, S.A., Collins, W.D., 2008. Radiative forcing by long-lived greenhouse gases: calculations with the AER radiative transfer models. J. Geophys. Res. 113.
Janjić, Z.I., 1990. The Step-Mountain coordinate: physical package. Mon. Weather Rev. 118, 1429–1443.
Janjić, Z.I., 1994. The Step-Mountain eta coordinate model: further developments of the convection, viscous sublayer, and turbulence closure schemes. Mon. Weather Rev. 122, 927–945.
Jia, W., Zhang, X., 2020. The role of the planetary boundary layer parameterization schemes on the meteorological and aerosol pollution simulations: a review. Atmos. Res. 239, 104890.
Kalabokas, P.D., Thouret, V., Cammas, J.-P., Volz-Thomas, A., Boulanger, D., Repapis, C.C., 2015. The geographical distribution of meteorological parameters associated with high

and low summer ozone levels in the lower troposphere and the boundary layer over the eastern Mediterranean (Cairo case). Tellus Ser. B Chem. Phys. Meteorol. 67, 27853.
Kalabokas, P., Jensen, N.R., Roveri, M., Hjorth, J., Eremenko, M., Cuesta, J., et al., 2020. A study of the influence of tropospheric subsidence on spring and summer surface ozone concentrations at the JRC ispra station in northern Italy. Atmos. Chem. Phys. 20, 1861–1885.
Kumar, A., Singh, D., Singh, B.P., Singh, M., Anandam, K., Kumar, K., et al., 2014. Spatial and temporal variability of surface ozone and nitrogen oxides in urban and rural ambient air of Delhi-NCR, India. Air Qual. Atmos. Health 8, 391–399.
Lee, J.-B., Cha, J.-S., Hong, S.-C., Choi, J.-Y., Myoung, J.-S., Park, R.J., et al., 2015. Projections of summertime ozone concentration over East Asia under multiple IPCC SRES emission scenarios. Atmos. Environ. 106, 335–346.
Li, L., Chen, C., Huang, C., Huang, H., Zhang, G., Wang, Y., et al., 2011. Ozone sensitivity analysis with the MM5-CMAQ modeling system for Shanghai. J. Environ. Sci. 23, 1150–1157.
Li, M., Liu, H., Geng, G., Hong, C., Liu, F., Song, Y., et al., 2017a. Anthropogenic emission inventories in China: a review. Natl. Sci. Rev. 4, 834–866.
Li, M., Zhang, Q., Kurokawa, J.I., Woo, J.H., He, K., Lu, Z., et al., 2017b. MIX: a mosaic asian anthropogenic emission inventory under the international collaboration framework of the MICS-Asia and HTAP. Atmos. Chem. Phys. 17, 935–963.
Li, K., Jacob, D.J., Shen, L., Lu, X., De Smedt, I., Liao, H., 2020. Increases in surface ozone pollution in China from 2013 to 2019: anthropogenic and meteorological influences. Atmos. Chem. Phys. 20, 11423–11433.
Lin, M., Fiore, A.M., Horowitz, L.W., Langford, A.O., Oltmans, S.J., Tarasick, D., et al., 2015. Climate variability modulates western US ozone air quality in spring via deep stratospheric intrusions. Nat. Commun. 6, 7105.
Lin, Y., Jiang, F., Zhao, J., Zhu, G., He, X., Ma, X., et al., 2018. Impacts of O3 on premature mortality and crop yield loss across China. Atmos. Environ. 194, 41–47.
Liu, Q., Lam, K., Jiang, F., Wang, T., Xie, M., Zhuang, B., et al., 2013. A numerical study of the impact of climate and emission changes on surface ozone over South China in autumn time in 2000–2050. Atmos. Environ. 76, 227–237.
Liu, H., Fu, M., Jin, X., Shang, Y., Shindell, D., Faluvegi, G., et al., 2016. Health and climate impacts of ocean-going vessels in East Asia. Nat. Clim. Chang. 6, 1037–1041.
Liu, H., Meng, Z.-H., Lv, Z.-F., Wang, X.-T., Deng, F.-Y., Liu, Y., et al., 2019. Emissions and health impacts from global shipping embodied in US–China bilateral trade. Nat. Sustain. 2, 1027–1033.
Londhe, A., Jadhav, D., Buchunde, P., Kartha, M., 2008. Surface ozone variability in the urban and nearby rural locations of tropical India. Curr. Sci. 1724–1729.
Lu, X., Zhang, L., Wang, X., Gao, M., Li, K., Zhang, Y., et al., 2020. Rapid increases in warm-season surface ozone and resulting health impact in China since 2013. Environ. Sci. Tech. Let. 7, 240–247.
Lu, X., Ye, X., Zhou, M., Zhao, Y., Weng, H., Kong, H., et al., 2021. The underappreciated role of agricultural soil nitrogen oxide emissions in ozone pollution regulation in North China. Nat. Commun. 12, 5021.
Luecken, D.J., Yarwood, G., Hutzell, W.T., 2019. Multipollutant modeling of ozone, reactive nitrogen and HAPs across the continental US with CMAQ-CB6. Atmos. Environ. 201, 62–72.
Lv, Z., Liu, H., Ying, Q., Fu, M., Meng, Z., Wang, Y., et al., 2018. Impacts of shipping emissions on PM2.5 pollution in China. Atmos. Chem. Phys. 18, 15811–15824.
Ma, M., Gao, Y., Wang, Y., Zhang, S., Leung, L.R., Liu, C., et al., 2019. Substantial ozone enhancement over the North China plain from increased biogenic emissions due to heat waves and land cover in summer 2017. Atmos. Chem. Phys. 19, 12195–12207.
Ma, M., Gao, Y., Ding, A., Su, H., Liao, H., Wang, S., et al., 2022. Development and assessment of a high-resolution biogenic emission inventory from urban green spaces in China. Environ. Sci. Technol. 56, 175–184.
Mellor, G.L., Yamada, T., 1982. Development of a turbulence closure model for geophysical fluid problems. Rev. Geophys. 20, 851–875.
Morcrette, J.J., Barker, H.W., Cole, J.N.S., Iacono, M.J., Pincus, R., 2008. Impact of a new radiation package, McRad, in the ECMWF integrated forecasting system. Mon. Weather Rev. 136, 4773–4798.
Morrison, H., Thompson, G., Tatarskii, V., 2009. Impact of cloud microphysics on the development of trailing stratiform precipitation in a simulated squall line: comparison of one- and two-moment schemes. Mon. Weather Rev. 137, 991–1007.
Murphy, B.N., Woody, M.C., Jimenez, J.L., Carlton, A.M.G., Hayes, P.L., Liu, S., et al., 2017. Semivolatile POA and parameterized total combustion SOA in CMAQv5.2: impacts on source strength and partitioning. Atmos. Chem. Phys. 17, 11107–11133.
Ni, Z.-Z., Luo, K., Gao, X., Gao, Y., Fan, J.-R., Fu, J.S., et al., 2019. Exploring the stratospheric source of ozone pollution over China during the 2016 Group of Twenty summit. Atmos. Pollut. Res. 10, 1267–1275.
Qu, H., Wang, Y., Zhang, R., Li, J., 2020. Extending ozone-precursor relationships in China from peak concentration to peak time. J. Geophys. Res. Atmos. 125, e2020JD033670.
Randerson, J.T., Van Der Werf, G.R., Giglio, L., Collatz, G.J., Kasibhatla, P.S., 2017. Global Fire Emissions Database, Version 4.1 (GFEDv4). ORNL Distributed Active Archive Center.
Rao, S., Klimont, Z., Smith, S.J., Van Dingenen, R., Dentener, F., Bouwman, L., et al., 2017. Future air pollution in the shared socio-economic pathways. Glob. Environ. Chang. 42, 346–358.
Riahi, K., van Vuuren, D.P., Kriegler, E., Edmonds, J., O'Neill, B.C., Fujimori, S., et al., 2017. The shared socioeconomic pathways and their energy, land use, and greenhouse gas emissions implications: an overview. Glob. Environ. Chang. 42, 153–168.
Saha, S., Moorthi, S., Wu, X., Wang, J., Nadiga, S., Tripp, P., et al., 2014. The NCEP climate forecast system version 2. J. Clim. 27, 2185–2208.
Sánchez, E., Yagüe, C., Gaertner, M.A., 2007. Planetary boundary layer energetics simulated from a regional climate model over Europe for present climate and climate change conditions. Geophys. Res. Lett. 34.
Shen, J., Zhang, Y., Wang, X., Li, J., Chen, H., Liu, R., et al., 2015. An ozone episode over the Pearl River Delta in October 2008. Atmos. Environ. 122, 852–863.
Sillman, S., 1999. The relation between ozone, NOx and hydrocarbons in urban and polluted rural environments. Atmos. Environ. 33, 1821–1845.
Situ, S., Guenther, A., Wang, X., Jiang, X., Turnipseed, A., Wu, Z., et al., 2013. Impacts of seasonal and regional variability in biogenic VOC emissions on surface ozone in the Pearl River Delta region, China. Atmos. Chem. Phys. Discuss. 13, 6729–6777.
Tan, Z., Lu, K., Jiang, M., Su, R., Dong, H., Zeng, L., et al., 2018. Exploring ozone pollution in Chengdu, southwestern China: a case study from radical chemistry to O3-VOC-NOx sensitivity. Sci. Total Environ. 636, 775–786.
Tang, G., Li, X., Wang, Y., Xin, J., Ren, X., 2009. Surface ozone trend details and interpretations in Beijing, 2001–2006. Atmos. Chem. Phys. 9, 8813–8823.
Tong, L., Zhang, H., Yu, J., He, M., Xu, N., Zhang, J., et al., 2017. Characteristics of surface ozone and nitrogen oxides at urban, suburban and rural sites in Ningbo, China. Atmos. Res. 187, 57–68.
Van Vuuren, D.P., Edmonds, J., Kainuma, M., Riahi, K., Thomson, A., Hibbard, K., et al., 2011. The representative concentration pathways: an overview. Clim. Chang. 109, 5.
Wang, Y., Shen, L., Wu, S., Mickley, L., He, J., Hao, J., 2013. Sensitivity of surface ozone over China to 2000–2050 global changes of climate and emissions. Atmos. Environ. 75, 374–382.
Xie, B., Fung, J.C.H., Chan, A., Lau, A., 2012. Evaluation of nonlocal and local planetary boundary layer schemes in the WRF model. J. Geophys. Res. Atmos. 117.
Xu, J., Tie, X., Gao, W., Lin, Y., Fu, Q., 2019. Measurement and model analyses of the ozone variation during 2006 to 2015 and its response to emission change in megacity Shanghai, China. Atmos. Chem. Phys. 19, 9017–9035.
Yan, F., Gao, Y., Ma, M., Liu, C., Ji, X., Zhao, F., et al., 2021. Revealing the modulation of boundary conditions and governing processes on ozone formation over northern China in june 2017. Environ. Pollut. 272, 115999.
Yang, G., Liu, Y., Li, X., 2020. Spatiotemporal distribution of ground-level ozone in China at a city level. Sci. Rep. 10, 7229.
Yang, J., Liu, M., Cheng, Q., Yang, L., Sun, X., Kan, H., et al., 2021. Investigating the impact of air pollution on AMI and COPD hospital admissions in the coastal city of Qingdao, China. Front. Environ. Sci. Eng. 16, 56.
Zhang, Y.H., Su, H., Zhong, L.J., Cheng, Y.F., Zeng, L.M., Wang, X.S., et al., 2008. Regional ozone pollution and observation-based approach for analyzing ozone–precursor relationship during the PRIDE-PRD2004 campaign. Atmos. Environ. 42, 6203–6218.
Zhang, Z., Zhang, X., Gong, D., Quan, W., Zhao, X., Ma, Z., et al., 2015. Evolution of surface O3 and PM2.5 concentrations and their relationships with meteorological conditions over the last decade in Beijing. Atmos. Environ. 108, 67–75.
Zhang, G., Gao, Y., Cai, W., Leung, L.R., Wang, S., Zhao, B., et al., 2019. Seesaw haze pollution in North China modulated by the sub-seasonal variability of atmospheric circulation. Atmos. Chem. Phys. 19, 565–576.
Zhang, L., Gao, Y., Wu, S., Zhang, S., Smith, K.R., Yao, X., et al., 2020. Global impact of atmospheric arsenic on health risk: 2005 to 2015. Proc. Natl. Acad. Sci. 117, 13975–13982.
Zheng, J., Zhong, L., Wang, T., Louie, P.K.K., Li, Z., 2010. Ground-level ozone in the Pearl River Delta region: analysis of data from a recently established regional air quality monitoring network. Atmos. Environ. 44, 814–823.
Zheng, B., Tong, D., Li, M., Liu, F., Hong, C., Geng, G., et al., 2018. Trends in China's anthropogenic emissions since 2010 as the consequence of clean air actions. Atmos. Chem. Phys. 18, 14095–14111.
Zhu, J., Liao, H., 2016. Future ozone air quality and radiative forcing over China owing to future changes in emissions under the representative concentration pathways (RCPs). J. Geophys. Res. Atmos. 121, 1978–2001.